한국표면공학회지
Journal of the Korean Institute of Surface Engineering
Vol. 31, No. 4, Aug. 1998
<연구논문>

Relationship between Pinned Wall Behavior and Surface Crystallization in Cobalt-rich, Near-zero Magnetostrictive Sensors

C. K. Kim and C. G. Yoo

Division of Materials Science and Metallurgical Engineering,
Hanyang University Haengdang-Dong,
Seongdong-Ku, Seoul, 133-791 KOREA

자왜계수가 0인 Co계 센서의 자벽 고착 거동과 표면 결정화간의 관계

김창경, 유충근

한양대학교 재료공학부

요 약

자벽고착 개념에 기초를 둔 새로운 조화센서는 다음과 같이 설명되어진다. 2단계 열처리된 Co계 비정질 precursor는 특이한 signal을 유발시키는데 이는 자속의 단계적인 변화를 나타내는 hysteresis loop에 기인한다. 자장하에서의 1단계 열처리는 M-H loop에서 일축 유도 자기이방성을 발생시킨다. 2단계 무자장하의 열처리는 고착된 자벽의 stepped hysteresis의 특성을 나타내는데 이로인해 유용한 marker로서의 특징을 가지게 된다.

열처리동안 비정질재료의 표면과 내부에서 상당량의 산화와 결정화 과정을 거치는 것이 관찰되었다. 이로인한 표면 자벽 고착 모델의 제안은 자벽의 고착이 비정질 부분과 semi-hard Co 층간의 접합면에서 가장 효과적으로 얻어진다는 것으로써 확신되어진다. 또한 자벽 고착 자장과 결정화된 Co층의 두께간의 상당한 연관성도 관찰되었다.

1. INTRODUCTION

Probably one of the most commercialized applications of amorphous magnetic materials is one as a sensor for electronic article surveillance (EAS), i.e., anti-theft security system. Electronic article surveillance systems are currently employed in super market, department store, libraries, video rental and other merchandise outlet stores, as well as to monitor everything such as workplace valuables from computers, diskettes to sensitive documents and even used as deterrent against infant abduction from hospital.

Such a security system consists of an elongated ferromagnetic marker (a tag, strip or label) which is attached to the merchandise or assets to be protected. These magnetic markers produce the non-linear hysteresis loops with non-linear permeability which are able to generate high order harmonics (n : 10-20) of the fundamental frequency and these can be detected as sharp voltage pulses by pick-up coils. When they are excited in field-generating coils arrayed around a passageway, the system is alerted. Such tags are called harmonic tags. The usage of this characteristic is not only limited to the anti-theft system but also applied to pulse generating sensor elements for rotary encoders, non-contact switchers, and various electric, magnetic sensors.

Since commonly available ferromagnetic materials do not generate such high order harmonics, the population of "false alarm" signals is low. Although other high quality ferromagnetic materials such as square permalloy[1] or "wasp-waisted" constricted Perminvar loop[2] can serve for such purposes, as well, they are less practical due to reduced reliability in service compared to the metallic glasses owing to their lower mechanical and magnetic stability which causes the degradation of their permeability during manufacture, dispensing and handling.

In order to fabricate these sensors, annealing of the amorphous ribbons under magnetic field is the crucial step to obtain unique signature in hysteresis loop. During annealing, it is observed that the surface and bulk of the amorphous material undergo substantial oxidation and crystallization. Thus the microstructure of the surface differs significantly from that of the bulk . These distinctive microstructures appear to be of critical importance for the performance of the harmonic tags. Hence, in this paper, the microstructural aspects of the tags are discussed. Also, attempts are made to correlate surface crystallization with macroscopic tag performances.

2. EXPERIMENT

A number of soft magnetic materials can be used as the precursor to the marker material. Usable materials are amorphous transition metal-metalloid compositions which include transition metals comprising Co and Fe with the total transition metal content 60 to 80 atomic percent and various combinations of metalloid contents (B and Si). These precursor amorphous alloys (general formula $Co_{95-x}Fe_5(BSi)_x$ were made by planar flow casting at the Metglas Products Division of Allied-Signal Corporation. Initial compositions were verified by chemical analysis with Auger electron spectroscopy (AES), X-ray photoelectron spectroscopy (XPS) and electron probe microanalysis (EPMA). These ribbons are characterized by near-zero magnetostriction ($(\lambda_s < 1 \times 10^{-6})$ and high dc permeability in the as-cast state. Differential scanning calorimetry indicates that the onset of crystallization occurs at 465℃ and maximum peak appears at 535℃.

Ribbons with a cross section of 20㎜×3㎜ were cut to a length of 40㎜. Samples were then first annealed under various time (3min.-7hrs.), temperature (250℃-420℃) and atmo-

sphere in the presence of a 60 Oe longitudinal magnetic field that saturated them along their length. Maximum annealing temperature was well below the crystallization temperature, 465 ℃. In this experiment, the second annealing was performed at temperature as low as 320℃ in a field free environment after the first annealing was done with a 60 Oe longitudinal field.

The field induced anisotropy was measured by hysteresis loop tracing after the first annealing. After the second annealing, the wall pinning force (average of left and right pinning force) vs. annealing time for different annealing temperature was measured by hysteresis loop tracing with a drive field of 1.5 Oe at 10 Hz. For the frequency domain analysis, the material was driven by a 73 Hz excitation from 0 to 2 Oe. The output level of the pick-up voltage at 1.5, 2.5, 3.5 and 8 kHz with a band width of 600 Hz was measured.

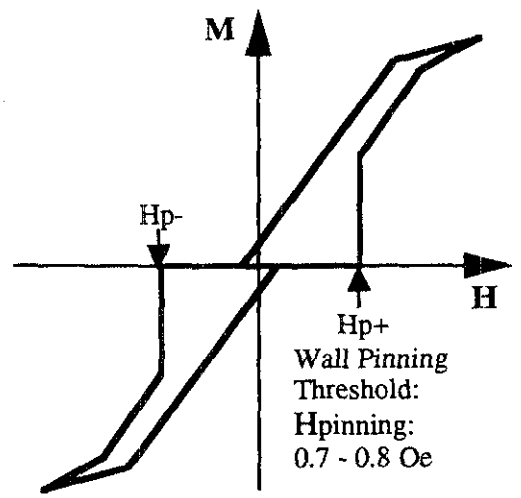

Fig. 1 Unique hysteresis characteristic with step changes in flux at threshold values of the applied field. Wall pinning threshold is indicated as $H_{pinning}$ (H_{P+} and H_{P-}).

3. RESULTS

3. 1 Fabrication of a pinned wall sensor

Harmonic sensors should generate the unique response signal when the sensor is subject to a magnetic field. One way to accomplish this is to obtain the hysteresis characteristic of the material which exhibits step changes in flux (reentrant magnetic flux reversal) at threshold values (Fig. 1). Then the permeability becomes highly non-linear and the high harmonic content in the voltage pulse is significantly increased. As a result, the sensor's response signal becomes more easily detectable over the lower frequency background noise and magnetic shielding noise which are often found to exist in EAS systems. This hysteresis characteristic is attributable to a domain wall configuration that remains pinned for increasing values of applied field up to the threshold value at which the pinned condition is disabled causing a step change in flux.

Annealing of the amorphous ribbons is the crucial step to obtain unique signature in M-H loop. These precursors undergo two step annealing procedures at wide ranges of time and temperature. The first annealing in the presence of a 60 Oe longitudinal magnetic field is performed to saturate ribbons along their length. This annealing causes a field induced anisotropy (offset) in M-H loop (Fig. 2). Then the ribbons are demagnetized to form magnetic domain walls. Subsequent annealing (the second annealing) under the absence of

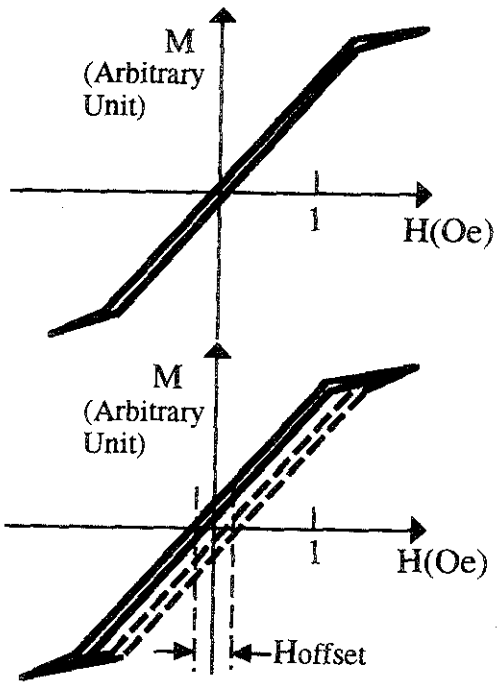

Fig. 2. M-H loops of $Co_{74.26}Fe_{4.74}Si_{2.1}B_{18.9}$ amorphous ribbon after field annealing and ac demagnetization (upper) and after positive (solid curve) and negative (dashed curve) field pulses of order 200 Oe.

magnetic field gives rise to the pinned wall stepped hysteresis characteristic which is indicative of the useful markers.

The deactivation of this marker is accomplished by exposing the marker to an ac decaying (degaussing) fields with maximum field amplitude from 50 Oe to 500 Oe in 50 Oe steps. During deactivation, additional domain walls are created in the marker and these walls remain in the marker after the marker is removed from the deactivating field. Consequently, the marker exhibits a different hysteresis characteristic leading to less pronounced step changes in flux or gradual changes in flux. It is possible to obtain an asymmetric magnetic reversal by biasing the marker with a small magnetic field (H=0.3 Oe) below the saturation level of the material during the second annealing. This is a special case of the previously described symmetric pinned wall loop obtained after the second annealing in a demagnetized state.

3.2 The effect of the microstructure on the domain wall pinning

We have found evidence that domain wall pinning is related to surface crystallization. Fig. 3 shows the wall pinning force ($H_{pinning}$) vs. annealing time for different temperature.

At low temperature such as 320℃, wall pinning with jittery switching threshold was observed. It is found that wall pinning force increases as the annealing time increases. For a given annealing time, the wall pinning force also increases with annealing temperature. It is observed that the wall pinning force in-

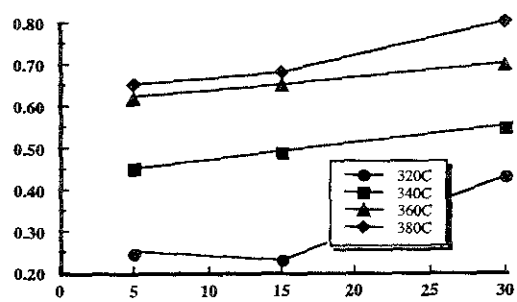

Fig. 3 Wall pinning force vs. annealing time after the second annealing. The first annealing is performed at 380℃ for 30 min. under the magnetic field of 60 Oe and the second annealing was performed at temperature as low as 320℃.

creases quite drastically from 320℃ to 360℃. It reaches a plateau above 360℃.

It is also observed that the wall pinning threshold of the resulting samples are very stable except for 320℃, 5 min. and 15 min. anneal. At 320℃, stable wall pinning is achieved with a longer time of 30 min. annealing. TEM study reveals that specimens annealed at 320℃ for 5 min. and 15 min. exhibit the partial crystallization of amorphous Co layer, while specimen annealed at 320℃ for 30 min. shows a fully crystallized Co layer. It is, therefore, believed that the semi-hard Co crystalline layer is necessary for the stabilization of the wall pinning. Annealing in N_2 and Ar at 380℃ for 60 min resulted in neither surface oxide formation nor Co crystallization, leading to no reentrant magnetization behavior. Etching of the surface faulted Co layer makes the wall pinning disappear, which again suggests that the wall pinning is associated the faulted Co crystalline layer. We also observed that there is a good correlation between pinning field and thickness of crystalline Co layer after the second annealing. According to Auger depth profile analysis, The semi-hard Co layer thickness grows in proportion to the borosilicate oxide layer thickness with an approximate relationship of $t_{\text{crystalline Co layer}} = 3.5\ t_{\text{surface oxide}}$.

We observed a strong relationship between the magnitude of the field induced anisotropy and the magnitude of the wall pinning threshold. Those which exhibited stronger field induced anisotropy after the first annealing resulted in more consistent and higher pinning threshold after the second annealing.

4. DISCUSSION

4. 1 Field induced anisotropy

Field annealing of polycrystalline or multiphase magnetic materials can lead to anisotropic microstructures which impose a magnetostatic anisotropy on the material[3-5]. In single and polycrystals and in amorphous materials the phenomenon of field induced anisotropy is often explained in terms of atomic pair ordering with a preferred direction imposed by the direction of magnetization[6-8]. There is abundant indirect evidence for pair ordering [9-12] based on the compositional dependence of induced anisotropy. For an alloy of two magnetic species A_xB_{1-x}, the field induced anisotropy often varies with composition like x(1-x) which reflects its dependence on A-B pair interactions; x(1-x) is the probability of finding an A-B pair in A_xB_{1-x}.

We can define the deviation of the ith bond direction or easy axis from its orientation in an isotropic distribution as $d\theta_i$. The net anisotropy energy density is related to the average of all $d\theta_i$s normalized by $4\pi : d\Omega/4\pi$, where $d\Omega = 1/N\Sigma_{i=1} d\theta_i$. A direct pair anisotropy of order $d\Omega/4\pi \mathbf{L} 10^{-3}$ is probably adequate to account for the strength of the observed induced anisotropy; thus such an anisotropic pair ordering is very difficult to observe directly by scattering experiments[6].

All of the current theories of directional ordering, however, consider only pairs of magnetic elements or transition metal-metalloid pairs[6-13]. It is not evident from these theories why a third element like oxygen does not con

tribute to directional ordering although the presence of oxygen to a certain degree is always detected in many alloy systems[14-16].

We observed an important contribution of oxygen to the response to heat treatment in a magnetic field. We found that oxygen caused impurity faults by condensing on the {111} planes of fcc Co crystal. There have been similar reports that field induced anisotropy in Ni-Fe-Co crystalline alloys of fcc structure (Perminvars) correlates strongly with the formation of oxygen impurity faults on {111} planes[17]. Nesbitt et al.[18] also reported that constricted hysteresis loops found in Perminvar after heat treatment were related to the oxygen impurity faults. According to them, diffraction experiments indicated that specimens having constricted loops had faults while those having normal loops did not. This observation is rarely discussed in texts on magnetic materials[3-5] but it was well documented in the literature[17-20]. This model applies also to the Permalloys[36] and to $Ni_{35}Fe$[20]. We are, therefore, surprised to find a similar correlation between the strength of field induced anisotropy, pinned wall reentrant magnetization behavior and the degree of faulting in the Co crystallized layer formed in annealed Co rich amorphous alloys.

4. 2 The mechanism of domain wall pinning

Aroca et al[21]. described the bulk pinning of domain walls in annealed amorphous alloys $Fe_{40}Ni_{40}P_{14}B_6$. Their ribbons were annealed with or without a field in order to develop a square loop or pinned wall loop. The shape, sign and strength of the wall pinning potential seen by a domain wall moving through a region of induced helical anisotropy during low-field or zero-field annealing has been described. They reported no microstructural studies on their samples. Their most important result for our present purpose was to show the difference in interaction potential between clockwise (+) and counterclockwise (-) walls with a clockwise induced helical anisotropy (IHA). They found that a domain wall of a given chirality interacts twice as strongly with an IHA of the same chirality as it does with one of the opposite chirality. Also the like-chirality interaction is at first repulsive, then more strongly attractive, while the unlike interaction is weakly attractive at all wall separations (Fig. 4). One important point emerging from their analysis and depicted in Fig. 13 is that for a domain wall to enter a like-chirality IHA requires a field proportional to W1; to free itself from this IHA requires a field proportional to W_1+W_2.

This may be related to what makes the wall pinning mechanism operate. Demagnetization of the ribbon by a decreasing ac field may send a random sequence of clockwise (+) and counterclockwise (-) chirality walls toward the clockwise (+) IHA. The former are more likely to get stuck and require the next nucleation event to be initiated from the edge or end of the ribbon; the latter are only weakly pinned in the IHA and will likely to be removed on the next half cycle. Thus a wall of the same chirality as the IHA is generally re-established upon demagnetization. Thus the wall pinning model suggested by them predicts the strength and sign of the potential

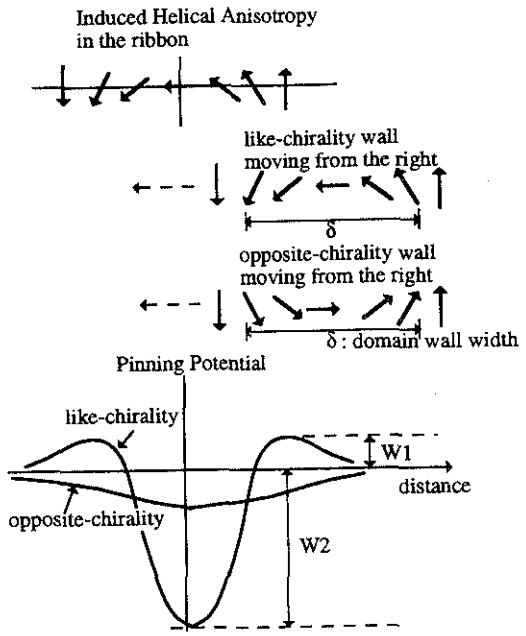

Fig. 4 Sketch of possible induced helical anisotropy in the bulk of a zero-field annealed magnetic material. Domain walls of the same chirality as the IHA will be strongly pinned because of their reduced magnetic anisotropy energy when they coincide with the IHA. On the other hand, domain walls have high energy at the position of an IHA of opposite-chirality.

seen by a domain wall moving through a region of IHA. However, the detailed nature of the pinning mechanism has been described as simple field induced helical anisotropy.

We explored the possibility that the flux jump in pinned wall sensor may be due to freeing the domain wall from its pinning potential rather than to nucleation of new walls at the ribbon edge or end suggested by Schafer et al[22, 24]. Three observations support the possibility of depinning the existing wall. First, a flux jump was detected in ribbons having two pinned walls. In this case, there is no need for wall nucleation at the sample edge, only at the end. Thus it is possible that the existing walls are freed (de-pinned) from their pinnings at the switching threshold ($H=H_{pinning}$).

Second, ribbons with widely differing edge or end roughness show almost consistent switching threshold ($H_{pinning}$). This would not be expected if edge or end domain wall nucleation were responsible for the flux jump. Third, the introduction of a semi-hard Co surface layer during annealing of the ribbons means that it is harder to move a pinned wall because it is now anchored at its ends in the semi-hard Co surface but it is much harder to nucleate a reversal domain at the ribbon edge because that process initiates completely within a semi-hard surface layer. However, we can not entirely exclude the possibility that pinned wall switching occurs due to nucleation and growth of reversal spike domains at the edge or the end of the ribbon as all the existing domain walls are pinned.

There are two possible models for the domain wall configuration in the ribbon right after demagnetization, i. e., just before the second anneal. We are convinced that the pinned wall may exist in a demagnetized ribbon not only in the center of the ribbon but also occur at the interface between the amorphous and semi-hard crystallized Co layers. It is important to point out that 180° domain wall straddles two layers (crystallized Co/amorphous Co) of different anisotropy. The wall pinning processes are considered as follows. The schematic of wall pinning modes

with and without surface semi-hard Co layer is shown in Fig. 5. The semi-hard crystalline Co layer is created during the first anneal and so is in a single domain state because of the field present during that anneal. During a demagnetization, however, the semi-hard surface layer still remains in the magnetized remanent state (remanent magnetization : 200 Gauss) due to a high anisotropic crystalline Co layer.

If we consider a simple bulk wall pinning model (Fig. 5a), a single vertical domain wall lies near the center of the ribbon (vertical domain wall), but displaced by d such that M =200 G. It is important to note that the vertical wall does not coincide with IHA. Since the wall is not pinned in IHA, the wall pinning strength is weak. However, if we consider the semi-hard Co surface layer created during the first magnetic annealing domain configuration can be differently depicted. With the surface wall pinning model (Fig. 5b), the amorphous interior supports a vertical wall as well as interfacial horizontal wall between the semi-hard layer and the soft amorphous layer. So from the perspective of the domain wall, the strength of wall pinning of the two states should be quite different. The stable wall pinning is obtained in a specimen with a surface Co crystallized layer shown in Fig. 5b since the interfacial wall pinning site provides much larger area for wall to be pinned at. Consequently, the vertical wall is not as strongly pinned as is the horizontal interfacial wall.

The cobalt-rich layer which is present during the second anneal appears to enhance its

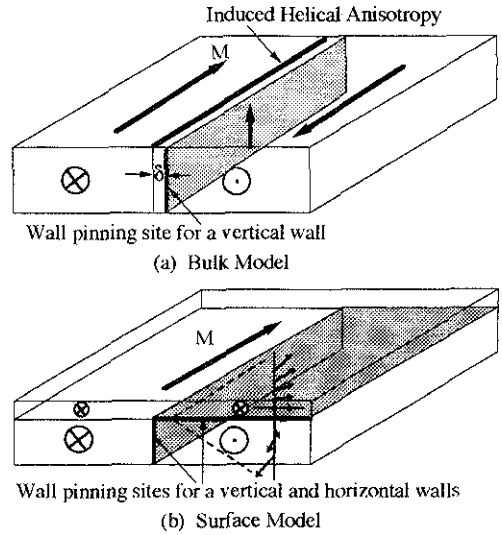

Fig. 5a. Bulk model : After demagnetization, tag is in a remanent state M>0 and a vertical domain wall is displaced by δ from the center of the ribbon. The displacement δ is exaggerated for clarity.

Fig. 5b. Surface model : After demagnetization, the surface semi-hard Co layer has remained magnetized. A vertical wall as well as interfacial horizontal wall between the semi-hard layer and the soft amorphous layer exists in the amorphous interior.

pinning efficacy. We speculate about the details of the mechanism by which this layer strengthens wall pinning during the second anneal. Possibilities include 1) further increase in cobalt layer crystallinity or thickness in the presence of the domain wall magnetostatic field, 2) more effective field induced anisotropy as oxygen impurity fault structure develops in cobalt layer, and 3) growth of the cobalt layer into the interfacial twist layer, resulting in its stabilization.

It is still not clear which microstructural features during annealing cause the induced

helical anisotropy (IHA) in the center of the ribbon. However, the annealing appears to induce a localized anisotropy around the vertical wall in the form of cobalt grain texture in the center of the ribbon. Therefore, we speculated that this localized texture may stabilize a vertical wall pinning.

5. CONCLUSION

By annealing a strip of cobalt-rich, near-zero magnetostrictive alloys, a novel type of a harmonic tag is fabricated. This marker exhibits a pinned wall hysteresis characteristic with a step change in flux at a threshold value of applied field. This hysteresis characteristic is attributable to a domain wall configuration that remains pinned for increasing values of applied field up to the threshold value at which the pinned condition is disabled causing a step change in flux.

During annealing, it is observed that the surface and bulk of the amorphous material undergo substantial oxidation and crystallization.

The domain wall pinning appears to be strengthened in the pre-grown semi-hard crystallized Co layer since the amorphous interior supports a vertical wall as well as interfacial horizontal wall between the semi-hard layer and the soft amorphous layer.

6. ACKNOWLEDGEMENT

The authors wish to acknowledge the financial support of Hanyang University, Korea, made in the program year of 1997.

REFERENCES

1. F. E. Luborsky, Amorphous Magnetism II (Plenum Press, New York, ed. by R. A. Levy and R. Hasegawa) Perspective on Application of Amorphous Alloys in Magnetic Devices, pp. 345-346, 1977.
2. S. Chikazumi, Physics of Magnetism (John Wiley & Sons, Inc., New York, ed. by S. Chikazumi and S. H. Charap) Chap. 14. The Irreversible Magnetization Process, pp. 291-301, Chap. 22. Kinds of Magnetic Materials, pp. 497-498, 1965.
3. S. Chikazumi, Physics of Magnetism (John Wiley & Sons, Inc., New York, ed. by S. Chikazumi and S. H. Charap) Chap. 17. Induced Magnetic Anisotropy, pp. 359-396, 1965.
4. S. Chikazumi and C. D. Graham Jr., Magnetism and Metallurgy (Academic Press, New York ed. by A. E. Berkowitz & E. Kneller) Chap. 12. Directional Order, pp. 577-619, 1969.
5. B. D. Cullity, Introduction to Magnetic Materials (Addison-Wesley, Reading MA, ed. by B. D. Cullity) Chap. 10. Induced Magnetic Anisotropy, pp. 357-376, 1972.
6. H. Fujimori, Amorphous Metallic Alloys (Butterworths, London, ed. by F. E. Luborsky) Chap. 16. Magnetic Anisotropy, pp. 300-316, 1983.
7. E. A. Nesbitt, R. Hasegawa, R. C. O'Handley and M. O. Sullivan, J. Appl. Phys., 51 (6) (1980) 3328-3329.
8. H. Fujimori, H. Morita, Y. Obi and S. Ohta, Amorphous Magnetism II (Plenum Press, New York, ed. by R. A. Levy and R. Hase-

gawa) On the Magnetically Induced Anisotropy in Amorphous Ferromagnetic Alloys, pp. 393-402, 1977.

9. T. Fukunaga and K. Suzuki, Sci. Rep. Res. Insts. Tohoku Univ., A29 (1981) 153 - 157.
10. F. E. Luborsky and J. L. Walter, IEEE Trans. Magn., MAG-13 (1977) 953-956.
    F. E. Luborsky and J. L. Walter, ibid., 1635-1638.
11. J. J. Becker, IEEE Trans. Magn., MAG-14 (1978) 938-940.
12. F. E. Luborsky and J. L. Walter, Mater. Sci. Eng., 28 (1977) 77-80.
13. P. Allia and F. Vinai, IEEE Trans. Magn., MAG-14 (1978) 1050-1053.
14. L. C. Feldman and J. W. Mayer, Fundamentals of Surface and Thin Film Analysis (North Holland, New York) Auger Electron Spectroscopy, pp. 269-274, 1986.
15. J. P. Chevalier, Y. Calvayrac, A. Quivy, M. Harmelin and J. Bigot, Acta metall., 31 (3) (1983) 465-471.
16. S. Chang and W. H. Wade, J. Phys. Chem., 74 (12) (1970) 2484-2488.
17. R. D. Heidenreich, E. A. Nesbitt and R. D. Burbank, J. Appl. Phys., 30 (7) (1959) 995 -1000.
18. E. A. Nesbitt, and R. D. Heidenreich, ibid., 1000-1003.
19. E. A. Nesbitt, R. D. Heidenreich and A. J. Williams, J. Appl. Phys., 31 (5) (1960) 228S-229S.
20. E. A. Nesbitt, B. W. Batterman, L. D. Fullerton and A. J. Williams, J. Appl. Phys., 36 (1965) 1235-1236.
21. C. Aroca, P. Sanchez and E. Lopez, Phys. Rev. B, 34 (1986) 490-493.
22. R. Schafer, W. K. Ho, J. Yamasaki, A. Hubert and F. B. Humphrey, IEEE Trans. Magn., 27 (1991) 3678-3689.
23. W. K. Ho and F. B. Humphrey, J. Appl. Phys., 63 (8) (1988) 2944-2946.
24. J. Yamasaki, K. Mohri, K. Watari, and K. Narita, IEEE Trans. Magn., 20 (1984) 1855 -1857.